J Intell Robot Syst (2012) 66:343–357
DOI 10.1007/s10846-011-9621-1

Image-Based Attitude Control of a Remote Sensing Satellite

Gregor Klančar · Sašo Blažič · Drago Matko · Gašper Mušič

Received: 29 December 2009 / Accepted: 13 July 2011 / Published online: 16 August 2011

Abstract This paper deals with the image-based control of a satellite for remote sensing. Approach is demonstrated by simulation where the position of the satellite is obtained with the Simplified General Perturbations Version 3 model and its orientation by simulating its dynamic and kinematic models. For a known position and orientation of the satellite the images are obtained using the satellite's onboard camera, simulated by the Google Earth application. The orientation of the satellite is governed by reaction wheels, which produce the required moments to the satellite. The image-based control law using SIFT image features is applied to achieve an automatic reference-point observation on the Earth's surface. Main contributions of the paper are the following: use of the same sensor for Earth observation and attitude control, simplicity of the approach, no need for explicit calibration of camera parameters and good tracking accuracy. Demonstrated simulation results and performance analysis confirm the approach applicability.

G. Klančar · S. Blažič · D. Matko · G. Mušič
SPACE-SI, Aškerčeva 12, Ljubljana 1000, Slovenia

G. Klančar · S. Blažič (✉) · D. Matko · G. Mušič
Faculty of Electrical Engineering,
University of Ljubljana, Tržaška 25,
1000 Ljubljana, Slovenia
e-mail: saso.blazic@fe.uni-lj.si

Keywords Satellite · Attitude control · Satellite kinematic model · Satellite dynamic model · Computer vision · SIFT features

Mathematics Subject Classifications (2010)
37N35 · 70B10

1 Introduction

In recent years, pico (less than 1 kg), nano (less than 10 kg) and micro (less than 100 kg) low-orbit satellites have become quite important in the space market. These satellites are much cheaper to build and to launch into Earth orbit, and also the development times (1 to 2 years) are much shorter compared to the highly capable, big and complex satellites. Such affordable missions offer the opportunity for different organizations to target specific applications and provide emerging space nations with independent Earth-observation facilities [14]. All these facts also make it possible for smaller players such as universities to obtain space technology, meaning it is no longer reserved only for big corporations. The primary role of such small satellites is Earth observation, which is usually done with a visual camera. Besides observation sensors, these small satellites also need attitude-determination sensors (e.g., sun sensor, earth magnetic sensor, star trackers, gyros, etc.), actuators for the satellites' attitude

correction (reaction wheels, small thrusters, magnetic coils, permanent magnets, etc.), a central computer and telecommunications. To utilize a broadband downlink and/or to observe the desired area on the Earth's surface, the satellite needs to have attitude control to achieve its desired orientation.

Earth-observation satellites need an attitude-control system to steer the satellite to the desired Earth-observation point. This can be easily solved by an operator at the ground station, who observes the camera image and controls the satellite's orientation (the human in the loop). However, such approaches are impractical and imprecise due to communication delays. Therefore, automatic attitude control is normally used, where the operator only controls the desired target area, while the satellite tracks it autonomously. Usually, Earth target tracking is solved using an extended Kalman filter in an attitude-localization unit, such as in [12] and [9], where estimates of the satellite attitude are obtained using relative and absolute sensor information. Such applications require navigation sensors (Earth magnetic, gyros, sun sensor and the like) and observation sensors (e.g., a camera). In these approaches, information from the camera is, therefore, not used in the satellite attitude control. However, there are some examples of satellite camera usage for automation purposes, such as satellite image registration or region-of-interest detection. The use of satellite camera image information for an automatic satellite image registration process was reported by [16] and [4], where feature pairs from sensed and reference images are identified. The compression of high-resolution JPEG satellite images using region-of-interest detection and coding by Fuzzy C-Means clustering is presented in [10].

On the other hand, a number of successful approaches in UAV (Unmanned Aerial Vehicle) localization and control were reported using camera and natural landmarks information. In [2] an improved version of the Scale Invariant Feature Transform (SIFT) is used for the navigation and safe landing of a helicopter. In [3] an analysis of different feature-extraction algorithms for the localization purposes of a quadrocopter are proposed. Vision-only navigation and the control of a small, autonomous helicopter using a Sigma-Point Kalman Filter is proposed in [1].

The main novelty of the presented work is image based attitude control approach for Earth observation satellites. The same camera is used for observation as well as for attitude control. Satellite orientation error is estimated and corrected by a proposed computer vision and visual servoing algorithm. The proposed approach has some important advantages as follows: simplicity of the approach due to the use of the same sensor for observation and attitude control, no need for explicit calibration of camera parameters and better tracking accuracy (compared to external attitude sensors performances). Considering the above mentioned advantages the proposed idea is especially attractive for small-satellite missions. The satellite achieves the desired Earth-observation spot using image-based control (visual servoing), which together with an onboard camera forms an attitude control loop. The proposed control uses only natural features (Scale Invariant Feature Transform—SIFT, [7]) to obtain the desired satellite attitude, which to the best of our knowledge is the first such approach to satellite attitude control. Visual servoing techniques are classified in to two main types: image-based control and position-based control. Image-based control uses features that are extracted from the image to directly provide control actions for actuators, as opposed to position-based control where the pose (attitude) of the object is firstly estimated from the image and then issued to pose-based control. In our case image-based control is more convenient to achieve a constant Earth-area observation because the control goal is not to directly achieve the reference satellite orientation given for all three Euler angles, but instead the goal is to control satellite orientation so that the desired Earth area is always in the image centre. In this work the mathematical models for determining the satellite position and orientation are implemented in the Matlab environment. They are used to simulate satellite motion in Earth orbit. From a known satellite position and orientation the satellite camera is simulated using the Google Earth application that provides camera images. Finally, these images are used to close the

control loop with the implemented image-based control.

The paper is organized as follows: In Section 2 the mathematical models of the position of the satellite, its orientation and camera focus point are given. The orientation of the satellite is governed by the image-based control law described in Section 3. The simulation results are presented in Section 4 and the conclusions are drawn at the end.

2 Mathematical Models

Mathematical models are needed to simulate a satellite's motion in Earth orbit (position and rotation) and its onboard camera operation. These models are a part of the simulation environment developed in this work.

In the following the mathematical models of the satellite's position, its orientation and camera focus point will be given. For the satellite position the Simplified General Perturbations Version 3 (SGP3) [5] is used. The orientation of the satellite is determined by its dynamic and kinematic models, while the calculation of the camera's focus point is a geometric problem. All these models are implemented in a Matlab-based satellite motion simulator.

2.1 SGP3 Model

The Simplified General Perturbations Version 3 model is used to simulate the satellite's position in its orbit, which is defined by the Kepler elements that describe the satellite's position at the initial time. The satellite's position at some arbitrary time can then be calculated as follows.

Given the Kepler elements of the orbit [13]

- i—inclination,
- Ω_0—Right Ascension of Ascending Node (RAAN) at epoch,
- ω_0—argument of perigee at epoch,
- M_0—mean anomaly at epoch,
- ε—eccentricity,
- n—mean motion

obtained from the NORAD two-line element set [13], where the epoch (initial time) t_0 and $\frac{1}{2}\frac{dn}{dt}$ are also given, the position of the satellite is then calculated as follows:

1. Calculate the mean anomaly M at time t

$$M = M_0 + n(t - t_0) + \frac{1}{2}\frac{dn}{dt}(t - t_0)^2 \tag{1}$$

2. Calculate (by iterations) the eccentric anomaly E from the mean anomaly using the Kepler equation

$$M = E - \varepsilon \sin(E) \tag{2}$$

3. Calculate the true anomaly φ

$$\varphi = \arctan\left[\frac{\sin(E)\sqrt{1-\varepsilon^2}}{\cos(E) - \varepsilon}\right] \tag{3}$$

4. Calculate the semi-major-axis a from the mean motion

$$a = \sqrt[3]{\frac{\mu}{n^2}} \qquad \mu = 3.986005 \cdot 10^{14} \tag{4}$$

5. Calculate the actual argument of perigee ω and RAAN Ω due to the geopotential coefficient $J_2 = 1.08263\ 10^{-3}$ [5]

$$\omega = \omega_0 + \frac{d\omega}{dt}(t - t_0) \tag{5}$$

$$\Omega = \Omega_0 + \frac{d\Omega}{dt}(t - t_0) \tag{6}$$

where

$$\frac{d\omega}{dt} = \frac{3}{4}n\left(\frac{a_E}{a}\right)^2 \frac{5\cos^2 i - 1}{(1-\varepsilon^2)^2} J_2 \tag{7}$$

$$\frac{d\Omega}{dt} = -\frac{3}{2}n\left(\frac{a_E}{a}\right)^2 \frac{\cos i}{(1-\varepsilon^2)^2} J_2 \tag{8}$$

and $a_E = 6378 \cdot 10^3$ is the semi-major-axis of the Earth ellipsoid.

6. Calculate the position of the satellite in the Earth Centered Orbit (ECO) frame

$$\mathbf{P}_{\mathrm{ECO}} = \begin{bmatrix} \frac{a(1-\varepsilon^2)\cos(\varphi)}{1+\varepsilon^2\cos(\varphi)} \\ \frac{a(1-\varepsilon^2)\sin(\varphi)}{1+\varepsilon^2\cos(\varphi)} \\ 0 \end{bmatrix} \tag{9}$$

7. Transform the ECO position into the position of the satellite in the Earth Centered Inertial (ECI) frame

$$\mathbf{P}_{\mathrm{ECI}} = \begin{bmatrix} \cos(-\Omega) & \sin(-\Omega) & 0 \\ -\sin(-\Omega) & \cos(-\Omega) & 0 \\ 0 & 0 & 1 \end{bmatrix} \times \begin{bmatrix} 1 & 0 & 0 \\ 0 & \cos(-i) & \sin(-i) \\ 0 & -\sin(-i) & \cos(-i) \end{bmatrix} \times \begin{bmatrix} \cos(-\omega) & \sin(-\omega) & 0 \\ -\sin(-\omega) & \cos(-\omega) & 0 \\ 0 & 0 & 1 \end{bmatrix} \mathbf{P}_{\mathrm{ECO}} \quad (10)$$

2.2 Dynamic and Kinematic Models of the Satellite

The dynamic and kinematic models of the satellite are as follows [13]:

$$\frac{d\boldsymbol{\omega}}{dt} = \mathbf{J}^{-1}(\mathbf{M} - \boldsymbol{\omega} \times (\mathbf{J}\boldsymbol{\omega})) \quad (11)$$

where $\mathbf{J}$ is the tensor of the satellite's moments of inertia, $\boldsymbol{\omega} = [\omega_u \quad \omega_v \quad \omega_w]^T$ is the vector of the angular velocities of the satellite with respect to the ECI frame (but expressed in the satellite frame), $\mathbf{M}$ are the moments applied to the satellite (expressed in the satellite frame) and $\times$ denotes the vector product.

As for kinematical model, we have, due to the simplicity of calculation, chosen the description with the Direction Cosine Matrix (DCM) $\mathbf{R}_{\mathrm{ECI}}^{\mathrm{Body}}$

$$\frac{d\mathbf{R}_{\mathrm{ECI}}^{\mathrm{Body}}}{dt} = \begin{bmatrix} 0 & \omega_w & -\omega_v \\ -\omega_w & 0 & \omega_u \\ \omega_v & -\omega_u & 0 \end{bmatrix} \mathbf{R}_{\mathrm{ECI}}^{\mathrm{Body}} \quad (12)$$

2.3 Calculation of the Focus Point

The line of sight of the camera is oriented in the z direction of the satellite co-ordinate system. The focus point on the surface of the Earth in the ECI co-ordinate system

$$\mathbf{F}_{\mathbf{ECI}} = \begin{bmatrix} x_f \\ y_f \\ z_f \end{bmatrix} \quad (13)$$

is then calculated from the intersection of the Earth's surface (it is supposed that the Earth is a sphere) and the line of sight

$$x_f^2 + y_f^2 + z_f^2 = R_E^2$$
$$\mathbf{P}_{\mathrm{ECI}} - \mathbf{D}d = \mathbf{F}_{\mathrm{ECI}} \quad (14)$$

where R_E is the Earth-sphere radius, $\mathbf{D}$ is the unit vector of the direction of the line of sight of the camera and d is the distance from the satellite position to the focus point. The system of four equations (14) with four unknowns (x_f, y_f, z_f, d) is solved analytically using the symbolic toolbox of Matlab. If the line of sight of the camera is in the direction of the Earth the system has two real solutions and the nearest to the satellite (smallest d) is used. In each step the actual position of the satellite ($\mathbf{P}_{\mathrm{ECI}}$) and the actual unit vector of the direction of the line of sight of the camera (oriented in the z direction of the Body co-ordinate system) in the ECI co-ordinate system

$$\mathbf{D} = \mathbf{R}_{\mathrm{ECI}}^{\mathrm{Body}^{-1}} \begin{bmatrix} 0 \\ 0 \\ 1 \end{bmatrix} \quad (15)$$

are used to calculate $\mathbf{F}_{\mathrm{ECI}}$. The focus point on the Earth in the Earth Centered Earth Fixed co-ordinate system (ECEF) is then calculated using

$$\mathbf{F}_{\mathrm{ECEF}} = \begin{bmatrix} \cos(\omega_E t) & \sin(\omega_E t) & 0 \\ -\sin(\omega_E t) & \cos(\omega_E t) & 0 \\ 0 & 0 & 1 \end{bmatrix} \mathbf{F}_{\mathrm{ECI}} \quad (16)$$

where t is the Greenwich Siderial Time and $\omega_E = 7.2921 \cdot 10^{-5}$ is the rotational rate of the Earth.

3 Image-based Control of the Satellite

Control of the satellite's orientation is performed using image-based (IB) control, where the simulated camera images are obtained from the Google Earth application. Successive images are compared based on extracted SIFT (Scale Invariant Feature Transform) features developed by [7]. The SIFT is convenient for image-feature generation in object-recognition applications [6] because they are invariant with respect to image translation, scaling, rotation, and partially invariant to illumination changes and affine or 3D projection.

In the proposed approach, at each frame the SIFT features are calculated and compared to the SIFT features from the reference image. The reference image is selected to cover the desired small area on the Earth that we want to continually observe. By comparing features from the current image with the features from the reference image the required control actions (reaction wheels) are determined to reorient the satellite to the reference focus point on the Earth's surface.

3.1 Capturing Images from Google Earth

We used Google Earth as an Earth's surface image generator and to simulate the satellite camera. The application has to be controlled from Matlab to reproduce the satellite view of the Earth's surface for a calculated satellite position and orientation. To achieve this Matlab connects to the ActiveX server interface of Google Earth, and then uses a part of the available properties and methods. Among others, the interface to the camera is available, which can be used to set the focus point as well as the range, tilt and azimuth of the camera. These properties are repeatedly set to match the desired focus point and satellite position during the simulation experiment. Once a proper image is displayed within the Google Earth render window, the image is captured by a call to a Matlab mex function written in C. Finally the acquired image is rotated to match the satellite orientation.

3.2 SIFT Features Generation

The SIFT feature locations in the image are calculated by comparing a sequence of the same, but scaled, images as follows [6, 7]. The image is sequentially filtered with the Gaussian kernel. The filtered images are subtracted from among each other to obtain the sequence of difference-of-Gaussian images. The smoothed images are then down-sampled and a new sequence of difference-of-Gaussian images is computed. This process is repeated until the image is too small for a reliable feature detection. Within the difference-of-Gaussian pyramid the maxima and minima for each sample point are detected by comparing the neighbours in the current image and the neighbours in the scale above and below. This procedure gives stable features according to the translation, scale, rotation and illumination conditions.

In this work the SIFT features were calculated using the toolbox [8], where each feature is represented by a descriptor vector with 128 elements and by a 4-element location vector. An example of the found SIFT features for a typical Google Earth image is given in Fig. 1. Each feature is shown with the location vector defined by the row and column image coordinates, the scale (vector size) and the orientation.

3.3 Feature Matching

For each sample time (defined by the camera frame rate) the current image features are matched to the reference image features so that each found pair of features represents the same point on the Earth's surface. The pairs are found by searching the feature space (descriptor). For each feature d in the current image a pair from the reference image d_r is found by searching for a minimal distance between them. To reduce the computational costs in Matlab this procedure is done by calculating the dot product of the normalized features ($|d| = |d_r| = 1$) as follows $d \cdot d_r = \cos\beta$, where β is the angle between the feature

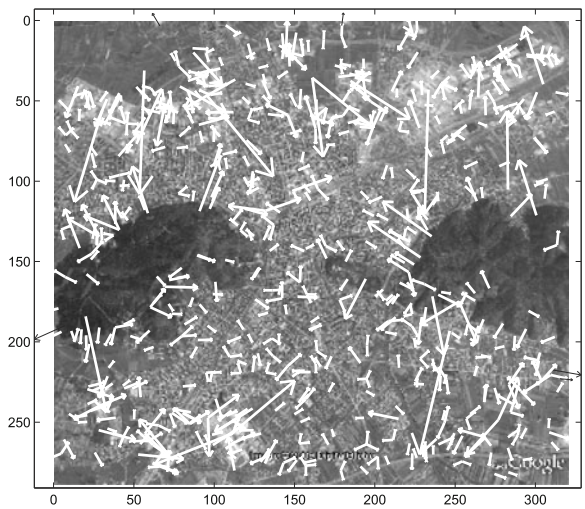

Fig. 1 SIFT features (*arrows*) found on the observed Earth image (in the 320×280 pixels image 729 features are found)

vectors d and d_r. For small angles β the distance among the features can be approximated by

$$|d - d_r| = D \approx \beta = \arccos(d \cdot d_r) \tag{17}$$

To increase the robustness, only pairs fulfilling the condition $\frac{D}{D_{\text{sec}}} < k$ are considered, where D is the distance among the features in the found pair, D_{sec} is the distance of the current feature to the second-nearest feature from the reference image and $0 < k < 1$ ($k = 0.6$). This means that the feature pairs are valid if no other feature is in the vicinity.

3.4 Image-based Control Algorithm

The relative satellite orientation according to the orbit frame [13] is usually described by three Euler angles: roll ϕ_O, pitch θ_O and yaw ψ_O. If $\phi_O = \theta_O = \psi_O = 0$ the Earth observation point is defined by the intersection of Earth's surface and the line between the satellite and the centre of the Earth.

To observe the desired point on the Earth's surface, the orbit frame is replaced by the reference frame, whose z axis points to the desired point on the Earth's surface (see Fig. 2). Then the satellite body's orientation is described according to the reference frame, which is described by the three Euler angles: the roll ϕ, pitch θ and yaw ψ. When these angles approach zero the satellite body frame aligns with the reference frame and the satellite z axis (camera) therefore points to the desired point on the Earth. This is achieved by setting ϕ and θ. The angle ψ must also be set so that the observed image from the camera does not rotate but maintains some reference image rotation (the image contents do not rotate). The desired point on the Earth's surface and the reference frame orientation are therefore defined by the reference image's centre and the rotation.

To meet the desired satellite orientation (attitude) the appropriate moments $\mathbf{M}$ (11) around the satellite body frame axes are calculated, depending on the orientation errors. These orientation errors are estimated from the found feature pairs between the reference and the current image. The error in the roll and pitch can be approximated from the estimated image translation $(\Delta x, \Delta y)$, while the yaw is related to the rotation $(\Delta\varphi)$ of the current image relative to the reference image.

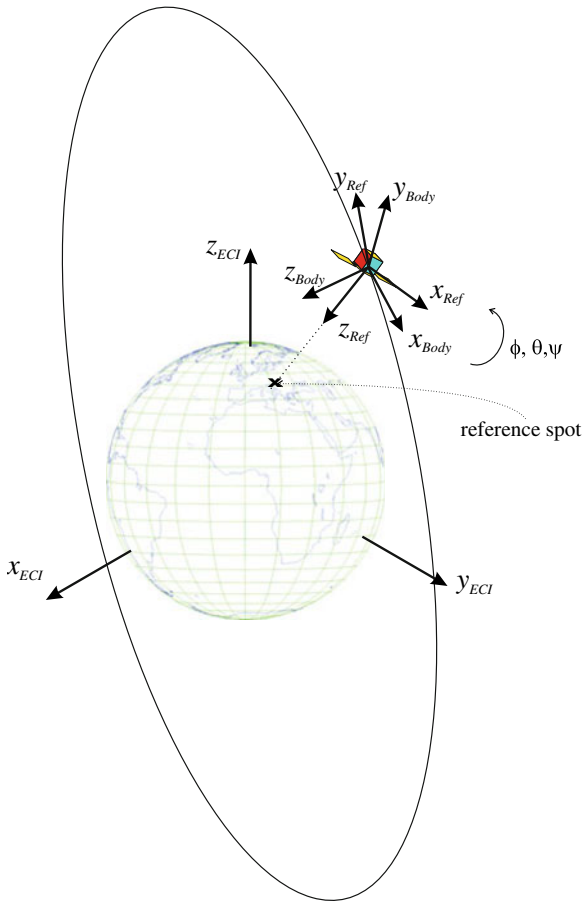

Fig. 2 Illustration of ECI, reference and body coordinate systems

The relation between the feature position in the reference image and the current image is as follows:

$$\begin{aligned} x_r &= \Delta x + x_c \cos\Delta\varphi - y_c \sin\Delta\varphi \\ y_r &= \Delta y + x_c \sin\Delta\varphi + y_c \cos\Delta\varphi \end{aligned} \tag{18}$$

where the indexes r and c denote the reference and the current image, respectively.

If the appropriate attitude control is applied to the satellite then the image observed from the satellite camera nearly aligns with the reference image. Of course, some orientation error $\Delta\varphi$ is to be expected, mostly due to image-sensor noise, different camera perspectives, camera lens distortions, and the like. Nevertheless, the orientation

error $\Delta\varphi$ is small, and therefore Eq. 18 can be simplified to

$$x_r = \Delta x + x_c - y_c \Delta\varphi$$
$$y_r = \Delta y + x_c \Delta\varphi + y_c \tag{19}$$

By defining the displacement $d_x = x_r - x_c$ and $d_y = y_r - y_c$ the relation (19) in matrix form is $\mathbf{D} = \mathbf{PT}$, where $\mathbf{D}_i = [d_{xi}, d_{y_i}]^T$, $\mathbf{T} = [\Delta x, \Delta y, \Delta\varphi]^T$ and

$$\mathbf{P}_i = \begin{bmatrix} 1 & 0 & -y_{ci} \\ 0 & 1 & x_{ci} \end{bmatrix}, \quad i = 1, \cdots, N$$

where $\mathbf{P}^T = [\mathbf{P}_1^T \cdots \mathbf{P}_N^T]$, $\mathbf{D}^T = [\mathbf{D}_1^T \cdots \mathbf{D}_N^T]$ and N is the number of feature pairs found in the current and the reference images. The best estimate for the error vector $\mathbf{T}$, considering all the feature pairs, is estimated using least squares

$$\mathbf{T} = (\mathbf{P}^T\mathbf{P})^{-1}\mathbf{P}^T\mathbf{D} \tag{20}$$

The transfer-function relation between the input moments $\mathbf{M}$ and the orientation (see Eq. 11) is, by its nature, a double integral. Therefore, the PD control structure is used as follows:

$$\mathbf{M} = \begin{bmatrix} k_{Px}\Delta x + k_{Dx}\dfrac{d}{dt}(\Delta x) \\ k_{Py}\Delta y + k_{Dy}\dfrac{d}{dt}(\Delta y) \\ k_{P\varphi}\Delta\varphi + k_{D\varphi}\dfrac{d}{dt}(\Delta\varphi) \end{bmatrix} \tag{21}$$

where k_{Px}, k_{Py}, $k_{P\varphi}$, k_{Dx}, k_{Dy} and $k_{D\varphi}$ are positive constants. Diagram of the proposed image-based attitude control algorithm is given in Fig. 3.

By the proposed image-based approach the calibration of intrinsic and extrinsic parameters of a camera is simple because the calibration is performed implicitly by tuning the controller parameters (21) (k_{Px}, k_{Py}, $k_{P\varphi}$, k_{Dx}, k_{Dy}, $k_{D\varphi}$) which result in the desired and stable operation. These controller parameters depend on intrinsic parameters (focal length of the camera and scale factors relating pixels to distance) but the latter are not required to be known and tuned explicitly. The calibration of extrinsic parameters (rotation and translation of the camera frame according to the main body frame) is not required because we control the view of the camera which is also used as orientation sensor. In case of position-based control implemented by some other orientation sensor (e.g. star tracker) also intrinsic parameters as well as extrinsic parameters (how satellite frame is related to the camera frame) need to be known. Therefore the proposed image-based approach enables much simpler calibration of the camera parameters compared to the position-based control implemented by some other external attitude sensor.

3.5 Classic Attitude Control

In this section the attitude control law using exact satellite attitude information (which is hard to obtain in practice) is developed for comparison purposes.

The satellite attitude is compared to the reference satellite attitude, both attitudes are expressed by their Euler angles (roll, pitch and yaw) according to the ECI frame. The reference satellite frame is placed in the satellite centre with the z axis oriented to the desired Earth spot area (Ljubljana city, see Fig. 2), while the x and y axes

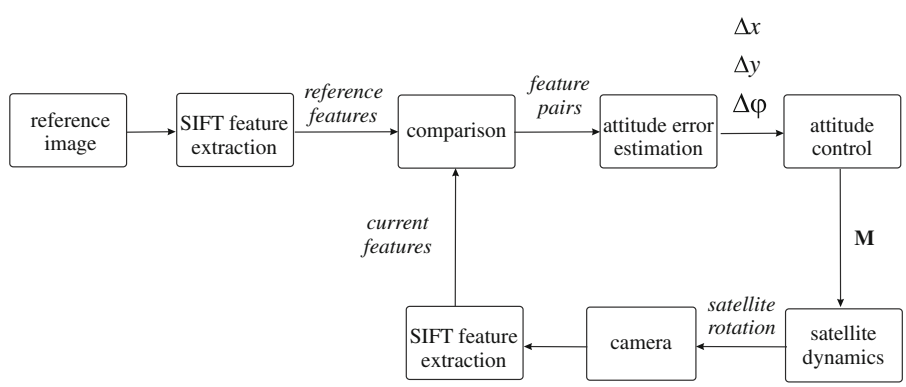

Fig. 3 Image-based attitude control algorithm diagram

are selected so that satellite camera image has the same orientation as the initial reference image.

In general, the rotation is defined by the rotation matrix (DCM) $\mathbf{R}_I^T$, which transforms the orientation vector in the initial frame ($\mathbf{v}_I$) to its representation in the target frame ($\mathbf{v}_T$) and is defined by $\mathbf{v}_T = \mathbf{R}_I^T \mathbf{v}_I$. This rotation can also be represented by the Euler angles ϕ, θ and ψ (roll, pitch and yaw). First, the initial frame is rotated around the x axis for ϕ, then the newly obtained frame is rotated around its y axis for θ, and, finally, the newly obtained frame is rotated around its z axis for ψ. These Euler angles are obtained from the rotation matrix R_I^T as follows

$$\begin{aligned} \phi &= \arctan2\left(\frac{\mathbf{R}_I^T(3,2)}{\mathbf{R}_I^T(3,3)}\right) \\ \theta &= -\arcsin\left(\mathbf{R}_I^T(3,1)\right) \\ \psi &= \arctan2\left(\frac{\mathbf{R}_I^T(2,1)}{\mathbf{R}_I^T(1,1)}\right) \end{aligned} \tag{22}$$

where arctan2 is the four-quadrant version of the inverse tangent function and (i, j) are the indexes in the rotation matrix $\mathbf{R}_I^T$.

In our case the rotation from the ECI to the satellite Body frame is defined by the $\mathbf{R}_{\text{ECI}}^{\text{Body}}$ rotation matrix (see Eq. 12) and by the Euler angles according to relation (22) ϕ_{Body}, θ_{Body} and ψ_{Body}. Similarly, the rotation from the ECI to the satellite reference frame is defined by the $\mathbf{R}_{\text{ECI}}^{\text{Ref}}$ rotation matrix and by the angles ϕ_{Ref}, θ_{Ref} and ψ_{Ref}. To determine the orientation-error angles between the satellite body frame orientation and the reference frame the rotation from the body to the reference frame is defined by the rotation matrix $\mathbf{R}_{\text{Body}}^{\text{Ref}} = \mathbf{R}_{\text{ECI}}^{\text{Ref}} \mathbf{R}_{\text{ECI}}^{\text{Body}\,T}$. The error angles e_ϕ, e_θ and e_ψ are then calculated from $\mathbf{R}_{\text{Body}}^{\text{Ref}}$ (see Eq. 22).

The attitude control is then obtained like in Eq. 21, as follows

$$\mathbf{M} = \begin{bmatrix} k_{P\phi} e_\phi + k_{D\phi} \dfrac{d}{dt}(e_\phi) \\ k_{P\theta} e_\theta + k_{D\theta} \dfrac{d}{dt}(e_\theta) \\ k_{P\psi} e_\psi + k_{D\psi} \dfrac{d}{dt}(e_\psi) \end{bmatrix} \tag{23}$$

where $k_{P\phi}$, $k_{P\theta}$, $k_{P\psi}$, $k_{D\phi}$, $k_{D\theta}$ and $k_{D\psi}$ are positive constants.

4 Simulation Results

The proposed image-based control is verified using the satellite simulator in the Matlab environment. The position, orientation and focus point of the satellite are determined as presented in Section 2. To obtain realistic images of the Earth during the satellite camera motion the Google Earth application is used to simulate the satellite's onboard camera. In the presented examples the Kepler elements of the satellite orbit are taken from the Lapan Tubsat [11] satellite, whose sun-synchronous orbit is approximately 600 km above the Earth's surface and needs approximately 90 minutes for one orbital period. The orbital speed of the satellite is approximately 7.5 km/s. The satellite's moment of inertia matrix $\mathbf{J}$ is set to be the unit matrix.

The simulator was designed and selected for the presented experiments because it is more convenient to design and test the control-law operation in a simulation environment. The current position and orientation can be easily obtained in a simulator and used to verify the operation of the controller. However, in the case of a real satellite the exact pose is hard to obtain, especially in the case of smaller satellites, which have a less precise attitude-determination system with fewer onboard sensors because of space limitations.

In the experiment the satellite must constantly observe the desired spot on the Earth's surface. This spot (Ljubljana city, in our case) is defined by the initial reference image taken at time $t_0 = 25$ s, where the initial time 0 is the time of the Kepler elements definition. Prior to t_0, the satellite is moving in its orbit with zero angular velocities and no attitude control, in such an orientation that at $t_0 = 25$ s the camera focuses on the desired Earth observation spot. After t_0 the reference spot is defined and the attitude control is switched on to enable a constant observation of that spot. The camera and attitude-control sampling frequency are fixed at 10 Hz and the camera resolution at 320×280 pixels. The ground sampling resolution of the Google Earth image varies among different

regions. The observed region in our case is covered by the resolution of 2.5 m/pixel. The obtained images were down-sampled to 15 m/pixel which is comparable to real camera systems in the LEO (low earth orbit) satellites where the resolution is typically 5–20 m/pixel [12].

In the following, the classic control is shown first, where the exact orientation data from the satellite motion simulator are used. Next the proposed image-based control operation is presented and evaluated.

4.1 Classic Control

The results of the simulation experiment using ideal attitude information are shown in Fig. 4, where the satellite body attitude is compared to the reference satellite attitude, both with respect to the ECI frame. In the experiment the satellite attitude is controlled using Eq. 23, where $k_{P\phi} = k_{P\theta} = k_{P\psi} = 0.1$ and $k_{D\phi} = k_{D\theta} = k_{D\psi} = 0.05$. Figure 5 shows the error in the Euler angles, which approach zero after some initial transition phase. This means that the satellite camera (z axis) focuses on the required spot on the Earth's surface. The initial transition phase appears because the satellite has zero angular velocities for all three axes at time t_0 when the attitude control starts. After the transition phase, when the satellite orientation errors approach zero, the appropriate satellite angular velocities are obtained,

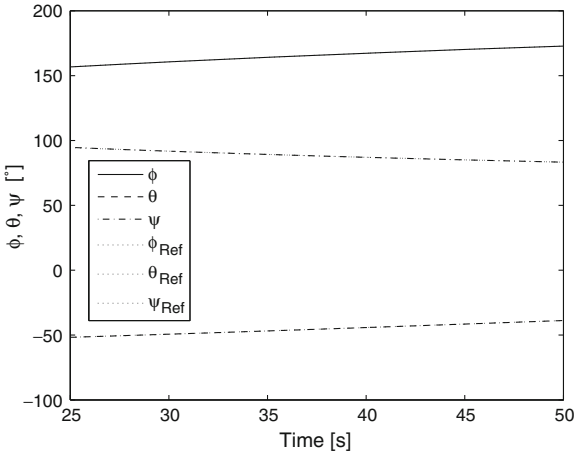

Fig. 4 Satellite body frame and reference satellite body frame Euler angles with respect to ECI frame

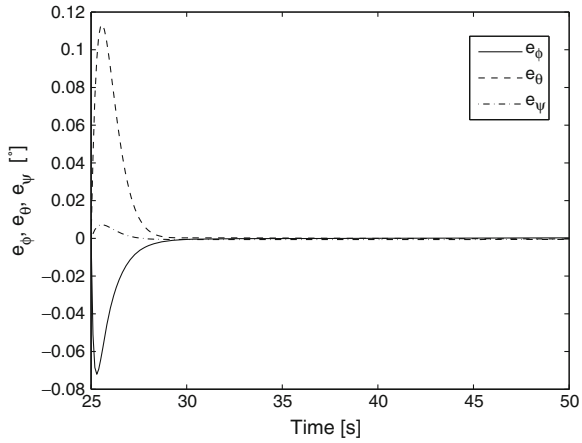

Fig. 5 The error angles during the classic attitude control

which enables constant tracking of the Earth reference spot. The moments applied to the satellite during the control are shown in Fig. 6. At the beginning of the experiment in Figs. 5 and 6 some overshoot appears due to the initial transition phase.

The reference Euler angles in Fig. 4 are approximately linear functions, with only a small contribution from the parabolic term and a negligible cubic-term contribution. The reference angles from Fig. 4 can be approximated by polynomials of the third order, as follows:

$$\phi_{\mathrm{Ref}}(t) = 3.0 \cdot 10^{-5}t^3 - 9.1 \cdot 10^{-3}t^2 + 1.2t - 24.6$$
$$\theta_{\mathrm{Ref}}(t) = -4.2 \cdot 10^{-5}t^3 + 6.5 \cdot 10^{-3}t^2 + 0.21t - 8.7$$
$$\psi_{\mathrm{Ref}}(t) = -3.6 \cdot 10^{-5}t^3 + 10.2 \cdot 10^{-3}t^2 - 1.0t + 19.5$$

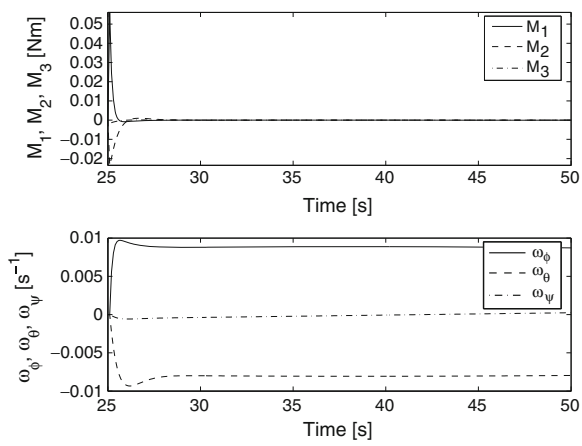

Fig. 6 Moments and angular velocities applied to the satellite during the classic attitude control

which means that the proposed controller structure (23) is appropriate for following the reference without any tracking error or with only a small, constant tracking error due to the small parabolic part. The integral part could also be added to the control (23) to cancel the tracking error if the reference angles have a higher parabolic contribution.

4.2 Image-based Attitude Control

As already mentioned, our goal is to control the satellite attitude using image sensor information only. In this section the simulation results using the proposed image-based attitude control (IB control) are presented. The proposed IB control (21) is used with $k_{Px} = k_{Py} = 2.5 \cdot 10^{-4}$, $k_{P\varphi} = 1.4$, $k_{Dx} = k_{Dy} = 1.5 \cdot 10^{-4}$ and $k_{D\varphi} = 1.8 \cdot 10^{-1}$.

The satellite path projection on the Earth's surface and the trajectory of the camera focus point for an uncontrolled satellite are shown in Fig. 7. Because no control is applied the satellite does not correct its orientation, and therefore the camera focus travels over the Earth's surface. In Fig. 8 the experiment with image-based control is shown. In this experiment the camera is focused on a fixed point on the Earth's surface that corresponds to the down-town of Ljubljana city. At the beginning of the experiment some overshoot appears. After this the camera focus point is quite stable. A small amount of noise is observed in the zoomed part of Fig. 8, which is due to the SIFT feature calculation and a least-squares estimation of the image translation and rotation.

The results of the image-based control are shown in Fig. 9, where the tracking errors Δx, Δy, $\Delta\varphi$ are indicated. These errors are obtained from comparisons of the current and the reference images using least-squares estimation (20). Some control-error oscillations are observed, which is due to the SIFT features' estimation and because the current images are observed with a different perspective, rotation and scale than the reference image. The moments applied to the satellite during control are shown in Fig. 10.

As already mentioned the SIFT features are quite robust to translation, rotation and scale in some reasonable area. However, if this area is exceeded (e.g., for rotations of $\pm 15°$) the estimated SIFT features are less reliable, which causes an increase in the attitude control error. Additionally, if the same scene as in the reference image is observed at a different perspective, the estimated image frame axes are not exactly the same as in the reference image. One of the reasons for this is perspective, which causes the reference axes

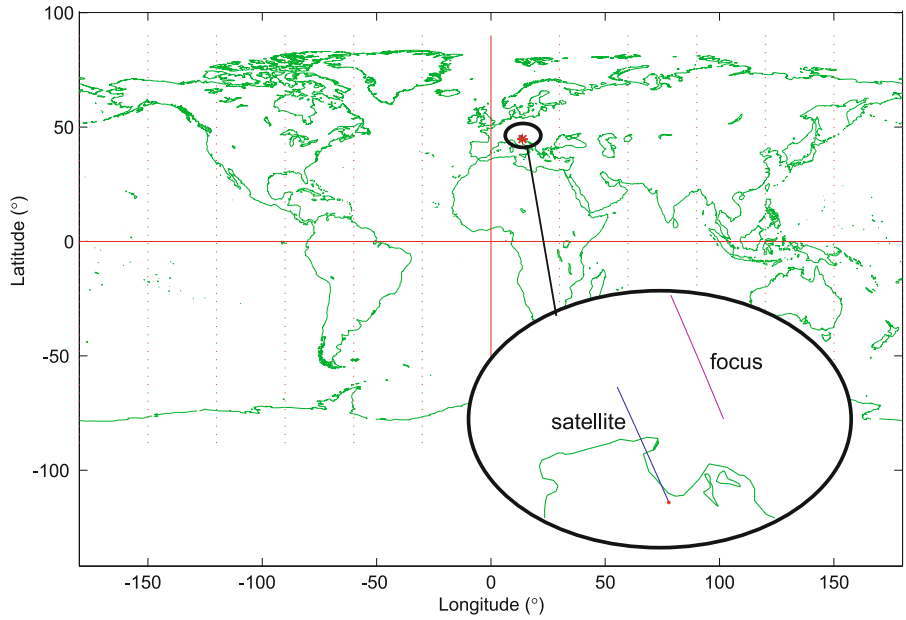

Fig. 7 Satellite motion and camera focus point without image-based control

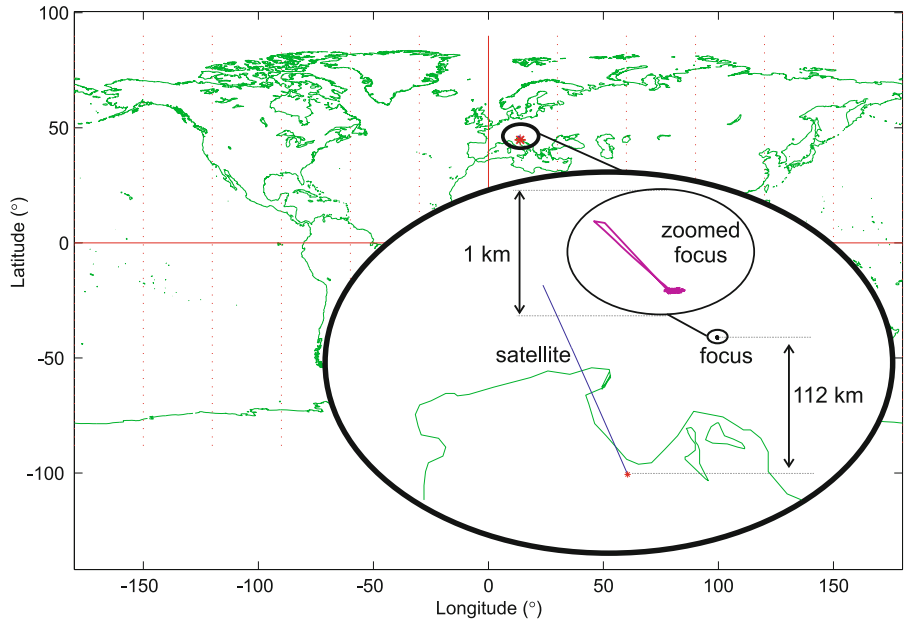

Fig. 8 Satellite motion and camera focus point with image-based control

(x and y) to be no longer perpendicular. The other reason could be the height of the reference Earth spot, which is not considered. The reference spot when observed from the side angle appears to be at a different position than it really is. The control tracking errors (Fig. 9) used in the IB control loop quickly approach zero, which confirms the correct and stable operation of the proposed control system.

A practical solution that increases the proposed IB control system's robustness to the SIFT features's estimation, perspective and some other unmodelled effects is the use of a moving reference. In the next experiment, in Figs. 11 and 12, the reference image is changed to the current image every $T_{ref} = 4$ s. The moments applied to the satellite during the control are shown in Fig. 11. Compared to the previous experiment (Figs. 9 and 10) the changes of rotation, scale, perspective and

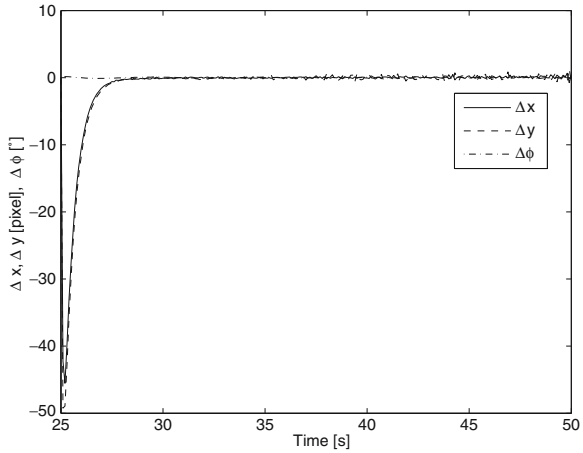

Fig. 9 Satellite IB attitude control. Tracking errors (translations Δx, Δy and rotation $\Delta\varphi$) between the reference image and the current image

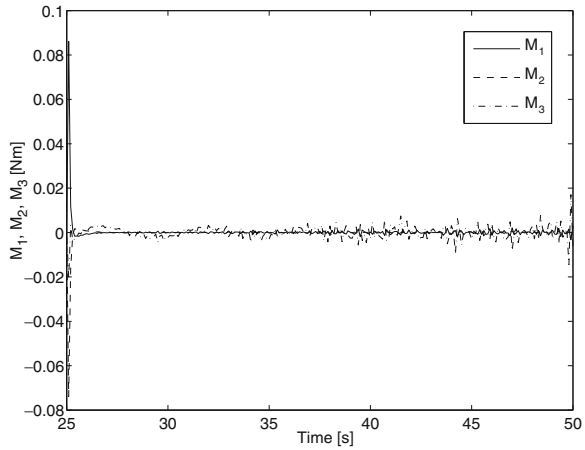

Fig. 10 Moments applied to the satellite during IB attitude control

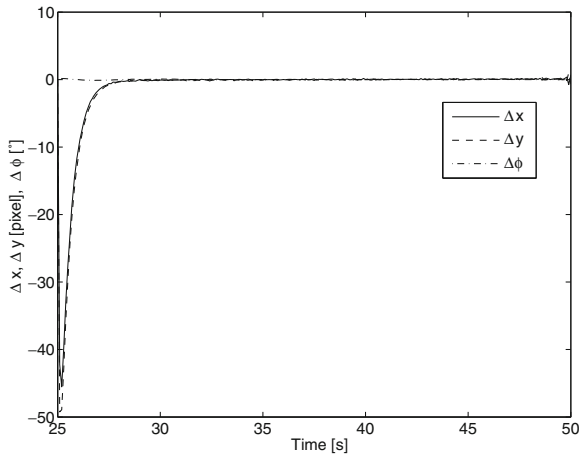

Fig. 11 Satellite IB attitude control with moving reference. Tracking errors (translations Δx, Δy and rotation $\Delta\varphi$) between the moving reference image and the current image

other influences have less effect on the attitude control error, while the quality of the tracking for the image centre and rotation do not change significantly. Also, the oscillations of the signals in steady state (Figs. 11 and 12) are lower and the time of the experiment can be much longer. In the previous experiment the satellite can focus on the reference spot until $t = 155$ s, after which the control fails because not enough reliable feature pairs can be found. In the case of the moving reference the control can reliably operate until the camera image has some useful content or until the camera

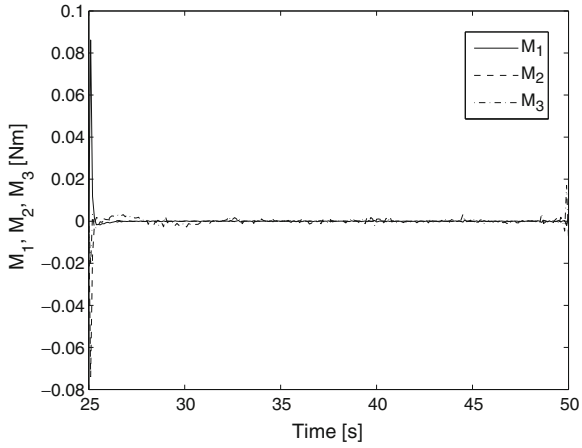

Fig. 12 Moments applied to the satellite during IB attitude control with moving reference

view to the reference spot becomes blocked by the Earth surface. The tracking errors are similar as in the fixed reference approach but the noise level is decreased and the robustness, operational time and approach applicability are increased. Because of many features pairs found (cca. 400 pairs) in the image the control tracking error is averaged and is sub pixel. According to Fig. 11 the control tracking error is 0.2 pixels which correspond to $3 \cdot 10^{-4}$ degrees or 3.1 m on the Earth surface. This means that obtained orientation of the camera view is quite stable with the image jitter less than 0.2 pixels.

To verify the operation of the proposed IB moving-reference control approach the comparison between the obtained satellite images and the ideal images is shown in Fig. 13. Ideal images would be obtained if the satellite focuses perfectly on the desired Earth spot. The desired Eart spot is defined by the centre of the first image taken at time $t_0 = 25$ s. Note that the goal of IB control is to force the translational and rotational errors obtained from Eq. 20 to zero. These average errors result from all the feature pairs found on the reference image and the current image. This is why it is not possible to define the error in the rotation for the whole image. Due to the change in the perspective different angles from the reference image are distorted in a very different way for the consequent images. In the IB control the rotation depends heavily on the direction containing more features. Nevertheless, the image content obtained from the camera is still very close to the ideal images, as seen in Fig. 13.

The satellite tracking errors ε_x and ε_y (according to the first image at $t = t_0$) at $t = 50$ s are approximately 2.5 pixels, which corresponds to a 37.5-m translation error that is hardly noticeable on the camera image (see Fig. 13). These conclusions can also be confirmed from Table 1, where the tracking errors ε_x, ε_y and their standard deviations (σ) for a fixed image reference (subscript $_f$) and for a moving image reference (subscript $_m$) are shown. Note that the rotation error is not shown due to the fact that it cannot be defined uniquely, as explained before. The tracking errors in Table 1 are evaluated according to the first image centre at $t = t_0$. As already explained the image distortions due to perspective and error

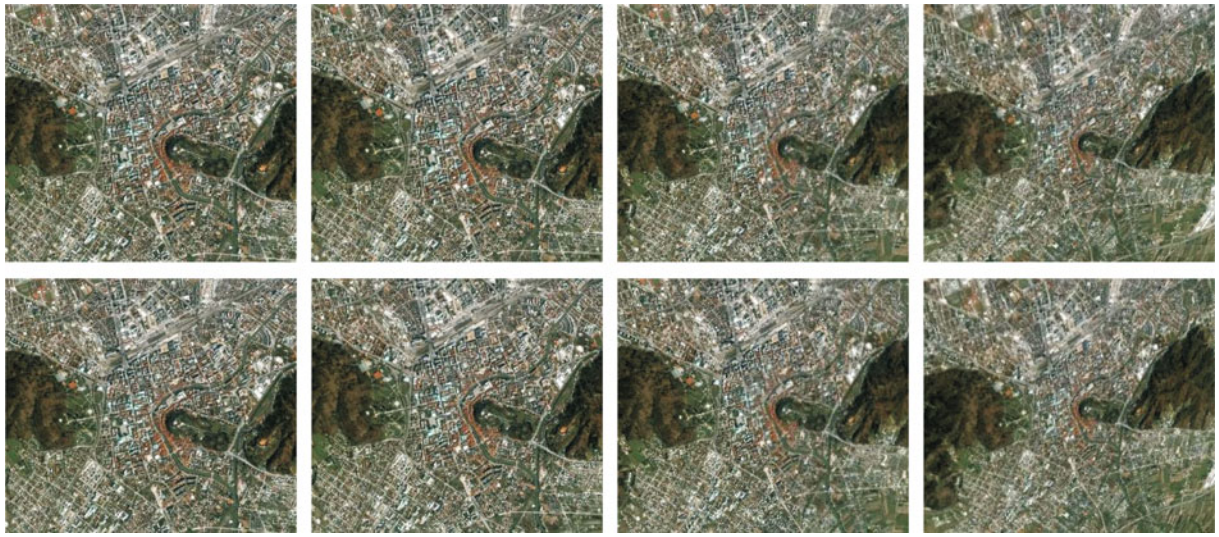

Fig. 13 Sequence of images during satellite motion. In the first row the images obtained with IB control and the moving reference are shown; they are taken at: 25 s, 50 s, 75 s and 100 s. In the second row the ideal images that would be obtained if the satellite perfectly tracks the desired Earth observation spot are shown; they are taken at: 25 s, 50 s, 75 s and 100 s

due to the lower SIFT feature reliability at higher rotation angles are not considered by transformation model (19). Therefore the center of the current image has some additional error according to the reference image center. The influence of these errors to the tracking accuracy of the current image center is analyzed in Table 1. At longer observation times the reference spot is observed by a higher tilt angle and the image becomes distorted because of a change in perspective. At times $t >$ 300 s the reference spot cannot be seen because the satellite view becomes blocked by the Earth (the hills around Ljubljana cover the city center). Nevertheless the estimated tracking error of the camera image center is approximately 2.5 pixels (for $t < 150$ s and moving reference approach) which corresponds to 37.5 m translation error. Note that this additional error does not make the proposed IB control unstable, because it is not included in the control tracking error (Fig. 11).

The approach with a moving reference can follow the desired Earth spot for a longer time (until $t = 300$ s, see Table 1). The number of found feature pairs (FP) between the reference image and the current image for the moving-reference approach is higher and more constant, which also explains the lower attitude-control error oscillations. A movie clip of the experiment can be seen at http://msc.fe.uni-lj.si/PublicWWW/Klancar/IBCmovie.html.

Table 1 IB control tracking performance comparison for the fixed ($_f$) and moving ($_m$) references

	30 s	50 s	100 s	150 s	200 s	250 s	300 s
ε_{xf} [pixel]	2	3	−7	−38	–	–	–
ε_{yf} [pixel]	−2	2	−3	−27	–	–	–
σ_{xf} [pixel]	0.06	0.35	1.18	17.54	–	–	–
σ_{yf} [pixel]	0.11	0.52	1.35	8.68	–	–	–
FP_f	500	350	160	16	–	–	–
ε_{xm} [pixel]	2	2	2	−9	−19	−26	−25
ε_{ym} [pixel]	0	4	−1	−8	−16	−20	−39
σ_{xf} [pixel]	0.04	0.34	0.04	0.39	0.11	0.13	12.90
σ_{yf} [pixel]	0.04	0.38	0.06	0.19	0.04	0.41	31.79
FP_m	460	640	470	345	364	204	26

Table 2 Performance evaluation of attitude control using external sensor (sun or star tracker sensor) and the proposed image-based (IB) strategy

Sensor	Sensor accuracy [°]	Control tracking error [pixel]	Control tracking error [m]
Sun sensor	0.1	90	1,440
Star tracker	0.001	1	16
IBC—feature tracking	–	0.2	3.3
IBC—image center tracking	–	2.5	40

4.3 Performance Evaluation of the IB Control Strategy

Here the performance of the proposed image-based attitude control and position-based attitude control with external sensor is analyzed. The obtained tracking results are compared to the expected accuracy of sun sensors and star tracker sensors that are usually used for attitude determination [12, 15]. The true orientation of the satellite (obtained from the simulator) was corrupted by the normal noise with standard deviation set according to the sun sensor expected accuracy (0.1°). To compare control tracking results the same feedback and PD controller gains are used as in the case of the proposed image-based control. The simulated sun sensor measurements therefore need to be scaled from radians to the pixels. This procedure enables us to figure out how the external sensor noise propagates to the tracking error in picture coordinates. The results of the attitude control performance analysis for sun sensor and star tracker external sensors are compared to the proposed image-based attitude control. The results are summarized in Table 2. The attitude control using sun sensor (usually combined with magnetometer) results in 90 pixels tracking error which corresponds to 1,340 m ground tracking error. Attitude control using star tracker sensor results in 1 pixel tracking error which corresponds to 15 m ground tracking error. As already evaluated the proposed image-based attitude control has 0.2 pixels tracking error noise which corresponds to 3.1 m ground tracking error noise. All these errors correspond to a 95% confidence interval. The estimated error of tracking the reference image center includes also the systematic error due to perspective and is 2.5 pixels or 37.5 m on the ground.

According to the analysis in Table 2 the expected accuracy (where both tracking and systematic errors are considered) of the image-based attitude control for tracking the reference image center is approximately 36 times higher and 2.5 times lower than the accuracy of sun sensor and star tracker, respectively. The proposed approach is therefore close to the star tracker sensor performance which is expensive, big and heavy (1 kg or more) and is therefore less appropriate for small LEO observation satellites.

5 Conclusion

The paper presents an approach to image-based control for a remote sensing satellite where the task is to control the satellite orientation so that the camera focuses on a reference point on the Earth's surface. A simulated environment was built with the complete modelling of the satellite kinematics and dynamics in order to simulate the satellite motion in the orbit. The camera image is simulated using the Google Earth application and SIFT features are used to implement image-based control. The SIFT features are appropriate for such a task because they are invariant to image translation, scaling, rotation, and partially invariant to illumination changes and an affine or 3D projection. They are, however, computationally demanding, which consequentially lowers the response time of the real-time control. A lower image resolution must be used; however, this increases the tracking error of the control. To improve the robustness of the proposed control to measurement noise, perspective, and other unmodelled effects, the concept of a moving reference is implemented. The obtained tracking performance is similar to the case with the fixed reference, while the performance regarding noise, robustness and operational time is greatly improved. The presented image-based control showed good performance in simulations with

realistic assumptions, so it could also be applicable to real satellite platforms. The results of the performance analysis show that the proposed approach accuracy is close to the performance of the star tracker sensor and much better than the expected accuracy of the sun sensor.

Acknowledgements The Centre of Excellence for Space Sciences and Technologies SPACE-SI is an operation partly financed by the European Union, European Regional Development Fund and Republic of Slovenia, Ministry of Higher Education, Science and Technology.

References

1. Bai, H., Wan, E., Song, X., Myronenko, A.: Vision-only Navigation and Control of Unmanned Aerial Vehicles Using the Sigma-Point Kalman Filter. ION NTM 2007, San Diego, CA, pp. 1264–1275 (2007)
2. Cesetti, A., Frontoni, E., Mancini, A., Zingaretti, P., Longhi, S.: A vision-based guidance system for UAV navigation and safe landing using natural landmarks. J. Intell. Robot. Syst. **57**(1–4), 233–257 (2010). doi:10.1007/s10846-009-9373-3
3. Erhard, S., Wenzel, K.E., Zell, A.: Flyphone: visual self-localisation using a mobile phone as onboard image processor on a quadrocopter. J. Intell. Robot. Syst. **57**, 451–465 (2010). doi:10.1007/s10846-009-9360-8
4. Fan, Y., Ding, M., Liu, Z., Wang, D.: Novel remote sensing image registration method based on an improved SIFT descriptor. In: Proceedings of SPIE, vol. 6790, pp. 67903G.1–67903G.6 (2007)
5. Hoots, F.R.: In: Roehrich, R.L. (ed.) Spacetrack Report No.3. Department of Commerce National Technical Information Service, Springfield VA (1988)
6. Se, S., Little, D.L.J.: Mobile robot localisation and mapping with uncertainty using scale-invariant visual landmarks. Int. J. Rob. Res. **21**(8), 735–758 (2002)
7. Lowe, D.G.: Distinctive image features from scale-invariant keypoints. Int. J. Comput. Vis. **60**(2), 91–110 (2004)
8. Lowe, D.: Demo software: SIFT keypoint detector. Available at http://www.cs.ubc.ca/~lowe/keypoints/ (2005)
9. Psiaki, M.L., Martel, F., Pal, P.K.: Three-axis attitude determination via Kalman filtering of magnetometer data. J. Guid. Control Dyn. **13**(3), 506–514 (1990)
10. Raj, E.S., Venkatraman, S., Varadan, G.: A fuzzy approach to region-of-interest coding in JPEG-2000 for ATR applications from high resolution satellite images. In: ICVGIP '08: Sixth Indian Conference on Computer Vision, Graphics & Image Processing, pp. 1993–200. IEEE Computer Society (2008). doi:10.1109/ICVGIP.2008.53
11. Renner, U., Buhl, M.: High precision interactive Earth observation with Lapan-Tubsat. In: Proceedings of the 4S Symposium Small Satellites, Systems and Services, Rhodos, Greece, 26–30 May 2008
12. Steyn, W.H.: A view finder control system for an earth observation satellite. Aerosp. Sci. Technol. **10**, 248–255 (2006)
13. Wertz, J.R.: Spacecraft Attitude Determination and Control. Reidel, Dordrecht (1978)
14. Wicks, A., Silva-Curiel, A., Ward, J., Fouquet, M.: Advancing small satellite Earth observation: operational spacecraft. In: Planned Missions And Future Concepts, 14th Annual AIAA/USU Conference on Small Satellites, pp. 1–8 (2000)
15. Wertz, J.R., Larson, W.J.: Space Mission Analysis and Design. Kluwer, Boston, MA (1999)
16. Wong, A., Clausi, D.A.: AISIR: automated inter-sensor/inter-band satellite image registration using robust complex wavelet feature representations. Pattern Recogn. Lett. (2010). doi:10.1016/j.patrec.2009.05.016